THE MULTIFRACTAL SPECTRUM OF THE DISSIPATION FIELD IN TURBULENT FLOWS

C. MENEVEAU and K.R. SREENIVASAN

Center for Applied Mechanics, Yale University, New Haven, CT 06520, USA

It has been pointed out (Mandelbrot 1974) that the turbulent energy dissipation field has to be regarded as a non-homogeneous fractal and that other more general quantities than the fractal dimension of its support have to be invoked for describing its scaling (metric) properties completely. This work is an attempt on amplifying this idea by using direct experimental data, and on making proper connections between the multifractal approach (described in section 2) and the traditional language used in the turbulence literature.

In the multifractal approach (Frisch & Parisi, 1983), the local behavior of the dissipation rate is described by a fractal power-law. We verify that this is so, and use it to measure the (infinite) set of 'generalized dimensions', and thus obtain the multifractal spectrum $f(\alpha)$ for one-dimensional sections through the dissipation field. Two operational approximations are made: first, for most of the results, a single component of the energy dissipation will be used as a representative of the total dissipation; second, we use Taylor's frozen flow hypothesis. The validity of both these approximations will be briefly assessed. We relate our results to lognormality, velocity structure functions, auto-correlation function of the dissipation rate, Kolmogorov's -5/3 law for the energy spectrum, the skewness and flatness factor of velocity derivatives, as well as to possible improvements in estimating various interface dimensions. We conclude that the multifractal approach provides a useful and unifying framework for describing the scaling properties of the turbulent dissipation field.

1. Introduction

For the study of fully developed turbulence it is necessary to provide a satisfactory description of the dissipation field of turbulent kinetic energy, which is highly intermittent (Batchelor & Townsend 1949). In an attempt to incorporate intermittency explicitly, Kolmogorov (1962) introduced the lognormal model. Several people - for example, Mandelbrot (1972), Kraichnan (1974) - have noted the inconsistencies present in the lognormal model. Mandelbrot (1974) introduced a fractal model in order to eliminate these inconsistencies. A simple version of this fractal model has become well known as the β-model (Frisch et al. 1978). The β-model has several shortcomings, one (by no means the most significant) of which is that it cannot account for the nonlinear behavior of the characteristic exponents of high-order velocity structure functions. To explain this

behavior in a consistent manner, Frisch & Parisi (1983) introduced the notion of a multifractal model.

In chapter 2 we shall review the Frisch-Parisi arguments using a nomenclature developed in the context of fractal attractors in phase-space and called the singularity spectrum, or the f-α curve (Halsey et al., 1986); we shall refer to that curve as the "multifractal spectrum". Note that, in the present work, the f-α curve refers to a multifractal description of the turbulent energy structure embedded in three dimensional physical space rather than in phase space. We then present in section 3 measurements determining the f-α curve for the dissipation field of turbulent energy. In sections 4 to 7 connections are highlighted between the experimentally determined f-α curve with several other descriptions such as the log-normality and a variety of scaling exponents. In section 8, we show that the multifractal spectrum correctly predicts the observed Reynolds number variation of the skewness and the flatness factor of velocity derivatives, while in section 9, we briefly discuss the corrections introduced for the fractal dimension estimates of surfaces such as the vorticity/no-vorticity interface. Section 10 contains some general conclusions.

2. Generalized dimensions and the multifractal spectrum: Theory

We start by observing (Frisch 1983) that the Navier-Stokes (N-S) equations

$$d\mathbf{V}/dt + \mathbf{V} \cdot (\nabla \mathbf{V}) = - \nabla(p/\rho) + \nu \nabla^2 \mathbf{V} \qquad (2.1)$$

are invariant under the following set of rescaling transformations:

$$\mathbf{r}' = \lambda \mathbf{r}$$

$$\mathbf{V}' = \lambda^{\alpha/3} \mathbf{V}$$

$$t' = \lambda^{1-\alpha/3} t \qquad\qquad (2.2)$$

$$(p/\rho)' = \lambda^{2\alpha/3} (p/\rho).$$

These rescaling transformations hold provided that $\eta < r, r' \ll L$ and $L \gg \eta$ (that is, in the high Reynolds number limit). Here η is the Kolmogorov microscale and L is a typical large scale imposed by external boundary conditions on the flow. The scaling exponent α is arbitrary, and cannot be

determined merely on grounds of dimensional analysis.

Next we focus our attention on how the dissipation behaves under these scale transformations. We use

$$\varepsilon_T \sim \delta v_r^{\,3}/r \tag{2.3}$$

to estimate the local dissipation of turbulent kinetic energy ε_r (averaged over a domain of size r); δv_r is some typical velocity difference across a distance r. The relation (2.3) is expected to be valid, essentially on dimensional grounds in the high Reynolds number limit, and is widely used in the turbulence literature. For an experimental justification of (2.3), see Sreenivasan (1984).

Using (2.2) we see that ε_r rescales according to

$$\varepsilon_r{}' = \lambda^{\alpha-1}\,\varepsilon_r\,. \tag{2.4}$$

From (2.2) we get $\lambda = r'/r$. Using for example r'=L and $\varepsilon_r{}' = \varepsilon_L$, we can write

$$\varepsilon_r = (\varepsilon_L/L^{\alpha-1})\ r^{\alpha-1} \sim r^{\alpha-1}\,. \tag{2.5}$$

Kolmogorov's original inertial range theory (Kolmogorov 1941) assumes no intermittency, that is that the locally averaged dissipation rate (a random variable in reality) is independent of the extent of the averaging domain. In the present notation, this is equivalent to saying that $\alpha=1$ in the complete three-dimensional space. The β-model assumes that the dissipation is confined to a homogeneous fractal subspace of the flow, of fractal dimension D_β. We shall see later that this model is equivalent to saying that α takes on the value D_β-2 on that homogeneous fractal.

The multifractal framework consists in supposing that α takes on different values on different interwoven fractal subsets of the three-dimensional physical space in which the dissipation field is embedded. The fractal dimension of the set with the scaling exponent lying between α and $\alpha + d\alpha$ will be denoted by $f(\alpha)$. This description will be shown to be general; among other things, it incorporates the intermittent behavior of the dissipation field (section 4) and is consistent with the nonlinear behavior of the exponents of the velocity structure functions (section 5). It also explains a number of other features (section 6-9).

Our first objective is to measure the f-α curve. For that purpose we analyze the scaling behavior of the total dissipation occurring in a d-dimensional box of size r

$$E_{r,d} \sim \epsilon_r \, r^d \sim r^{\alpha-1+d} \quad . \tag{2.6}$$

Now we divide the d-dimensional space in boxes of size r and sum powers of different order q of $E_{r,d}$ (q real) over all boxes. If the dissipation of turbulent energy is a multifractal, we expect these sums to scale with the size of the boxes r according to some power law. If we write that

$$\sum E^q_{r,d} \sim r^{(q-1)D_q} \tag{2.7}$$

the quantity D_q defines the so-called generalized dimensions (Hentschel & Procaccia, 1983; Halsey et al. 1986; in the context of probability measures these exponents are also called Renyi dimensions). Using equation (2.6) we can write (2.7) as

$$\sum r^{(\alpha-1+d)q} \sim r^{(q-1)D_q}. \tag{2.8}$$

Next we approximate the sum on the left-hand side of equation (2.8) by an integral over all possible values of α (for details, see Halsey et al. 1986). Note that we use $\alpha-1+d$ where these authors use α, both expressions being equivalent if local isotropy of the multifractal is assumed, but the former bears a closer relationship to the rescaling transformation (2.2) with which we started. (Let us also note that the assumption of local isotropy does not hold exactly for the turbulent dissipation field, but it will be assumed as working condition for the rest of this work for the sake of simplicity. A more thorough discussion will be given elsewhere.) The integrand must be weighted by the number of boxes for which α takes on values between α and $\alpha+d\alpha$. If iso-α sets are fractals with fractal dimension $f_d(\alpha)$, this weight is clearly $\rho(\alpha) \, r^{-f_d(\alpha)}$, where $\rho(\alpha)$ is a density. Therefore

$$\int \rho(\alpha) \, r^{(\alpha-1+d)q-f_d(\alpha)} \, d\alpha \sim r^{(q-1)D_q} \quad . \tag{2.9}$$

Now one uses the method of steepest descent to extract the dominant term from the integral in the limit of small r, and obtains

$$\rho(\alpha)[2\pi/|f''(\alpha)|]^{1/2} \, (\log r)^{-1/2} \, r^{(\alpha-1+d)q \, - \, f_d(\alpha)} \sim r^{(q-1)D_q} \tag{2.10a}$$

$$\text{if} \quad \partial f_d/\partial \alpha = q \quad \text{and} \quad \partial^2 f_d/\partial \alpha^2 < 0 \quad . \tag{2.10b}$$

Taking the logarithm of equation (2.10a) and neglecting log(logr)/logr as r

tends to zero one can write

$$(\alpha-1+d)q \; - \; f_d(\alpha) \; = \; (q-1) \; D_q \; . \tag{2.11}$$

or

$$f_d(\alpha) \; = \; \alpha q \; - \; (q-1)(D_q-d+1) + d -1. \tag{2.12a}$$

Differentiating (2.11) with respect to q we get

$$\alpha \; = \; d/dq[(q-1)(D_q-d+1)] \tag{2.12b}$$

The last two identities allow the calculation of α and its corresponding $f_d(\alpha)$ once the function D_q is known, and it is this function which can be determined in practice. For homogeneous fractals one has that D_q is a constant equal to the fractal dimension of the support, and does not depend on q. It is interesting to note that $D_q=3$ for Kolmogorov's original theory (Kolmogorov, 1941), and therefore (from 2.12 with d=3) we have $\alpha=1$ and $f(1)=3$. The multifractal spectrum thus consists of a single point. For the β-model we have $D_q=D_\beta$ and again (with d=3) we get a single point in the multifractal spectrum at $\alpha=D_\beta-2$ and $f(D_\beta-2)=D_\beta$.

Furthermore, equations (2.12) allow us to obtain some interesting results concerning the behavior of the generalized dimensions D_q under intersections with lower-dimensional spaces, and this question is addressed in appendix A. In the next section we focus on the special case of linear intersections of the dissipation field, that is d=1. If D_q and $f(\alpha)$ are the generalized dimensions and multifractal spectrum of these linear sections, we can write

$$\alpha \; = \; d/dq[(q-1)D_q] \tag{2.13}$$

$$f(\alpha) \; = \; \alpha q \; - \; (q-1)D_q. \tag{2.14}$$

These are the results we shall use in our experimental determination of the f-α curve.

3. Generalized dimensions and multifractal spectrum: Experiments

In this section, we analyze several fully developed turbulent flows (two dimensional wakes and boundary layers, nearly homogeneous and isotropic turbulence behind grids, and atmospheric boundary layer) in the manner described above. We base our analysis on measured time series of

the streamwise velocity component $u_1(t)$. We use Taylor's hypothesis and suppose that the time series can be considered as a linear cut through the 'frozen' turbulent velocity field in the streamwise direction (say x_1-axis). Furthermore, we suppose that the square of gradients in only one direction are representative of the actual dissipation, ε. A few remarks on the validity of these approximations will be made in Appendix B. For the rest of the analysis, it will be assumed that $(du_1/dt)^2$ represents features of the dissipation field, and will be normalized by its own mean.
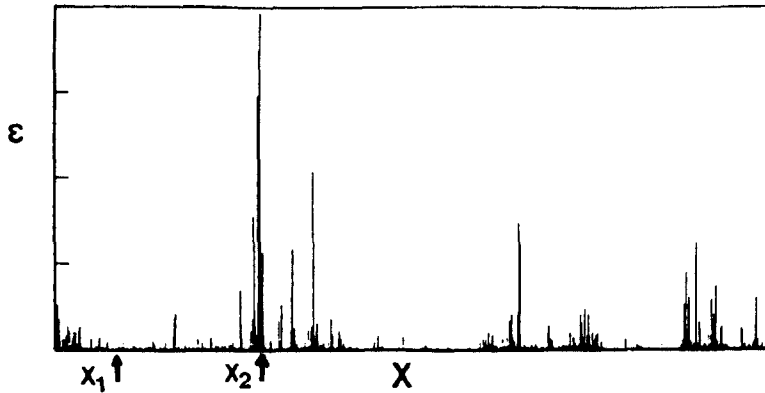
Figure 1a. Typical time trace of $(\partial u_1/\partial t)^2$, representative of the rate of dissipation of turbulent kinetic energy.
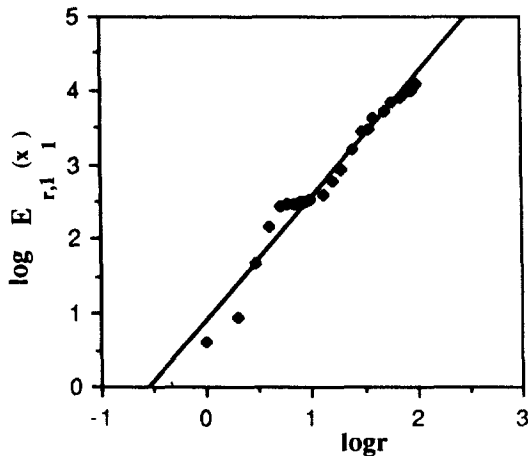
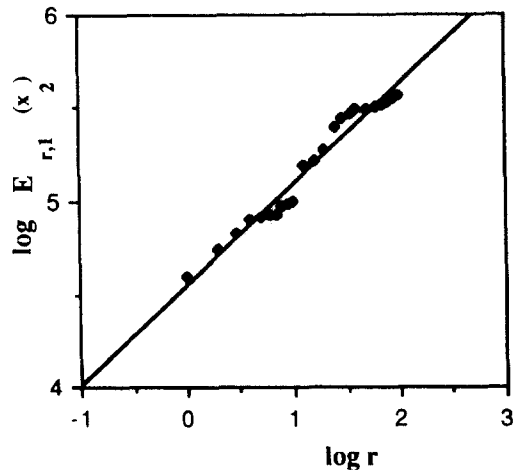Figure 1b. Local power-law behavior of E_r around x_1 (arbitrary units).

Figure 1c. Local power-law behavior of E_r around x_2 (arbitrary units).

Figure 1a shows a typical distribution of $\varepsilon \sim (du_1/dt)^2$ as a function of position (or time) along the intersecting line. It is clear that the signal is highly intermittent. We can also verify that local power-laws like (2.6) exist by identifying linear regions in plots of log $E_{r,1}(x_i)$ vs log r, where $E_{r,1}(x_i)$ is the total dissipation contained in a region of size r centered around some point x_i. The slope will be equal to α. Figures 1b and 1c show such plots for two different locations x_1 and x_2 (marked with arrows in figure 1a), the first corresponding to a region of low-dissipation and the second to a region where the dissipation is very intense. By fitting straight lines to figures 1b and 1c we get that $\alpha = 1.65$ for x_1 and $\alpha = 0.54$ for x_2. As will be shown later in this section, these values are close to the maximum and minimum values of α.

It is now straightforward to divide the x-axis into segments or boxes of size r and calculate E_r for each box as the area under $(du_1/dt)^2$, and then perform the sum of $E_r{}^q$ over all boxes. Let us call this sum Z. That is,

$$Z = \Sigma \ E_r{}^q \ . \tag{3.1}$$

This calculation is repeated for different values of r, and log $Z^{1/(q-1)}$ is plotted vs log r. In general these plots will show a linear region somewhere in the inertial range, the slope being D_q.

A question of some importance in measuring the D_q exponents is the convergence of Z. By convergence of Z we mean that Z/s tends to a constant, where s is the size of the domain used to evaluate Z. Usually s has to be extremely large to achieve convergence especially for large q, this being a well known problem in calculating high-order moments in turbulence (see for example Frenkiel & Klebanoff 1975; Sreenivasan et al. 1978).

In the context of numerically generated fractals (for example by iterating nonlinear maps), the number of points available for the calculations is limited only by computer size. In general, by incrementing the number of points on the fractal, the range of scaling is also incremented (because smaller and smaller scales become available when generating more iterations on a nonlinear map).

In our experimental situation, however, where an inner and outer cutoff of scaling is present and is fixed, say η_k and L, the excessive increase of data points (which corresponds to longer duration, if the sampling frequency is kept constant) corresponds to analyzing sets that are excessively larger than the outer cutoff scale L.

To clarify the arguments, let n = s /L, that is, n is the ratio between

the size of the domain used to calculate   Z, and L. Let l be the total length of the set available from an experiment and call m=l /s .   S is a proper subset of L. Figure 2 shows the different sets L(i), S(j) and L ,   whose sizes are L,s , and l respectively. The union of n consecutive L(i)-sets gives a S(j)-set, and the union of m consecutive S(j)-sets is the total set L available from experiments (that is, complete time series). Equivalently, the following relations hold :

and

$$U_{i=jn}^{i=j(n+1)} L(i) = S(j) \qquad j=1,2,....,m$$

$$U_{j=1}^{m} S(j) = L \qquad (3.2)$$
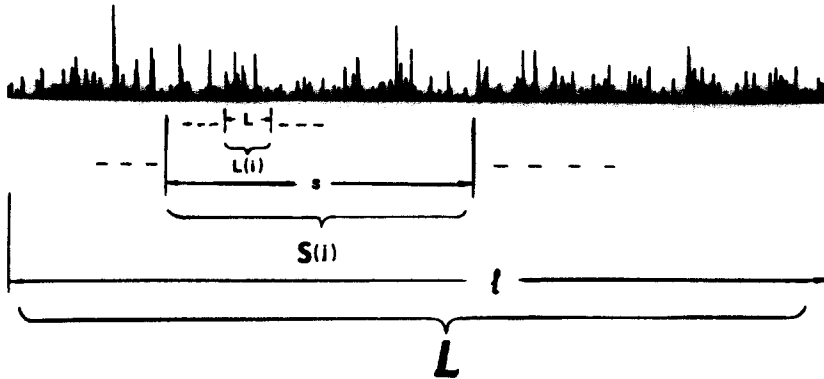
Figure 2. Definition of different subsets of the dissipation field and their relative size.

Suppose that $D_q(i)$ are the generalized dimensions of the set L(i). If we now perform the sum Z over a large S(j)-set, that is, n is taken very large (say 500) to ensure convergence, it is possible that the power-law dependence of Z with r gets degraded due to small fluctuations in $D_q(i)$, η_k and L from one L(i) to another. This may in general result in less defined straight lines and in shorter scaling ranges in the plots of log $Z^{1/(q-1)}$ versus log r.

On the other hand, if we use small n, say n=50, convergence is not achieved, and Z changes from one S(j) to another for a given r. In a given S(j)-set, however, the power-law dependence holds generally better under the circumstances than if n is large, allowing convincing estimates to be

made of the corresponding slopes to determine $D_q(j)$. But, as already pointed out, these $D_q(j)$ possess fluctuations from one $S(j)$ to another. We have reasons to believe that these fluctuations are due in part to local anisotropy of the turbulent dissipation field. This field consists (as seen in flow visualizations) of convoluted sheets rather than of spherically symmetric clusters. The values of D_q for high q can depend on the angle with which those sheets (the most intense ones) intersect the measuring probe. This explanation for the observed fluctuations is based on our preliminary studies, and our efforts in this direction are continuing.

In practice, therefore, one can either measure the D_q-exponents for a high number of short sets (low n and high m) and then average the results, or a low number of longer sets (high n and low m). In the first case one deals with little uncertainty when determining the slopes, but with a higher variance from one set to another. In the second case, the variance gets smaller, but the uncertainty in determining slopes gets larger. This situation was also observed in the context of fractal surfaces of iso-velocity and iso-dissipation, as reported in Sreenivasan & Meneveau (1986).

A generally valid compromise is hard to find and the precise nature of the described trend varies from case to case. In our measurements in wakes, grid and boundary-layer turbulence, it was generally preferable to use low values of n (30-75), since it was not possible to identify straight regions for high n. Even for the low n used in those cases, approximately 10% of the $S(j)$ were not taken into account because there was no convincing linear region.

In the case of atmospheric turbulence (where L is hard to estimate, but is usually very large) the use of "long" time series was highly satisfactory and in fact allowed unambiguous identification of linear regions between scales ranging over 3 to 4.5 decades. We analyzed 5 different time series, each of which is 30 seconds long. Even though about 2.10^5 data points were available for calculating Z, strict convergence was not achieved due to the low value of n (large value of L). We observed again fluctuations in the measured D_q from one set of data to another, the variance being very similar to that for the laboratory flows. On the other hand, there was virtually no uncertainty in fitting the slopes of the linear regions over 3 to 4.5 decades.

Having outlined the primary experimental difficulty one encounters while trying to measure the set of D_q-exponents, we present the results using in each case some appropiate value of n. Table 1 contains the flow description for each case, where we indicate the parameters n and m used in the measurement of the corresponding D_q.

Table 1

	Laboratory boundary layer	Grid turbulence	Wake of a cylinder	atmospheric boundary layer
Symbol:	$\triangle$	$\diamondsuit$		$\blacklozenge$
Position of hot-wire	$y/\delta = 0.4$ boundary layer thickness : $\delta = 11.4$ cm	$x/M=40$ Mesh size : $M=1.27$ cm Solidity = 0.44	$x/d=100$ Cylinder dia.: $d = 1.8$ cm $y/\delta = 1.3$ half-wake thickness: $\delta = 3.8$ cm	height $h = 2$ m above the roof of a 4-story building
Free stream velocity U_∞ (m/s)	12.2	14	15	Mean velocity at hot-wire location = 6 m/s
Convection velocity at hot-wire location U_c(m/s)	10.6	14	14.55	6
rms velocity-fluctuations u' (cm/s)	66	30	42	42 ($\pm 30\%$)
Taylor micro-scale λ (cm) $\lambda^2 = u'^2 U_c^2/<\acute{u}^2>$	0.48	0.35	0.32	5.3
Reynolds number $R_l = U_\infty l / \nu$	93,000 $l=\delta$	12,000 $l=M$	18,000 $l=d$	$8 \cdot 10^5$ $l=h$
$R_\lambda = u' \lambda / \nu$	209	70	90	1,500 ($\pm 30\%$)
Kolmogorov micro-scale η_k (mm) $\eta_k = \{\nu^2 U_c^2/15<\acute{u}^2>\}^{1/4}$	0.27	0.21	0.17	0.7 ($\pm 7\%$)
longitudinal integral length-scale L (cm)	3.6	1.9	3.9	$> 18,000$
Data-aquisition frequency (Hz)	20,000	30,000	40,000	6,000
n (see text)	40	75	30	1
m (see text)	5	5	5	5

Figure 3 shows some typical plots of log $Z^{1/(q-1)}$ vs log(r) for several values of q for the case of boundary layer turbulence in a wind-tunnel. Linear regions can be identified over a scale range of 1.5 to 2 decades. Figure 4 illustrates the case for atmospheric turbulence where linear regions can be identified over 3 to 4.5 decades (see appendix C).
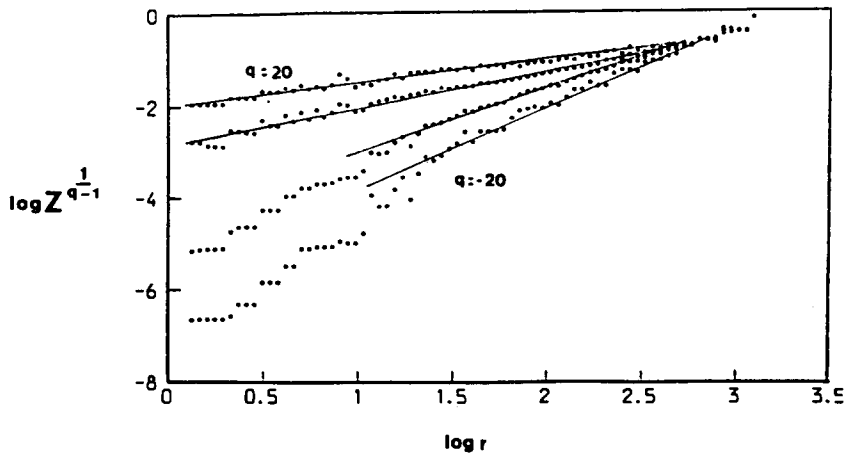

Figure 3. Typical plots of log $Z^{1/(q-1)}$ versus log r for the dissipation field measured in a turbulent boundary layer in a wind tunnel. Linear regions are visible over 2 decades for q>0 and over 1.5 decades for q<0. (Z and r in arbitrary units.) q=20,2,-2 and -20, from top to bottom.
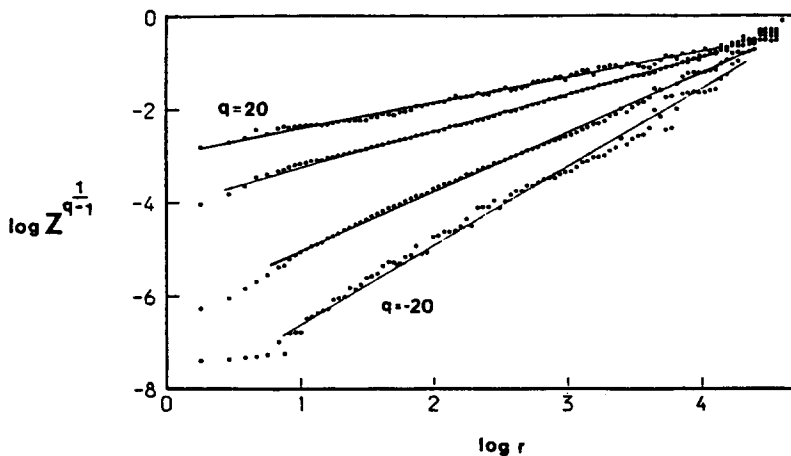
Figure 4. Typical plots of log $Z^{1/(q-1)}$ versus log r for the dissipation field measured in the surface layer of the atmosphere. Linear regions are visible over 4.5 decades for q>0 and over 3 decades for q<0.
(Z and r in arbitrary units.) q=20,2,-2 and -20, from top to bottom.

Figures 5 to 8 show the resulting D_q - curves for each different flow. The scatter and the error bars represent the variations of D_q from one S(j) to another, and the typical uncertainty in determining the slopes in the $\log Z^{1/(q-1)}$ vs log r plots, respectively.
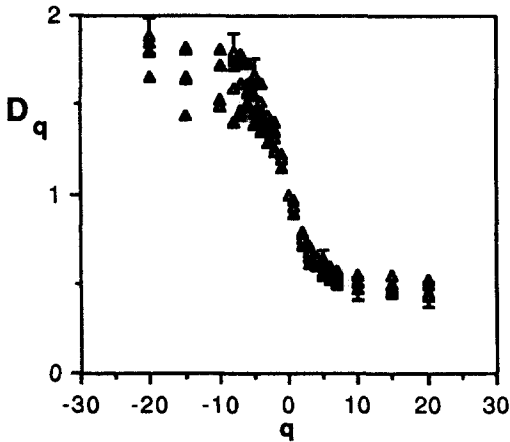
Figure 5. Generalized dimensions D_q as a function of q for 5 different subsets S(j) of the dissipation field measured in a wind tunnel turbulent boundary layer.
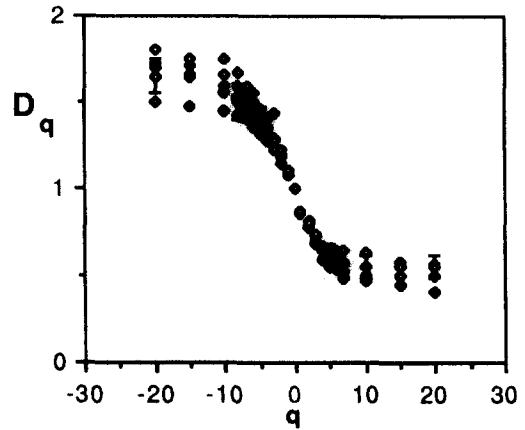

Figure 6. Generalized dimensions D_q as a function of q for 5 different subsets S(j) of the dissipation field measured in the turbulent flow behind a grid.
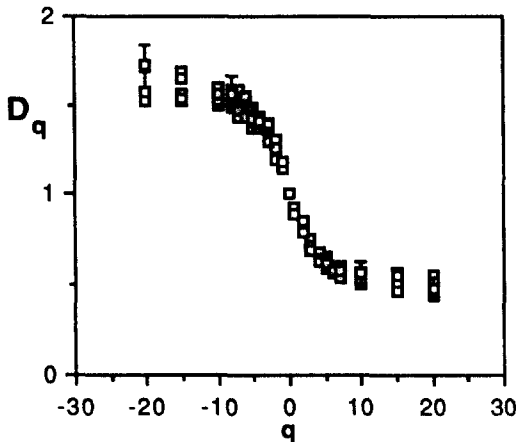

Figure 7. Generalized dimensions D_q as a function of q for 5 different subsets S(j) of the dissipation field measured in the turbulent wake behind a circular cylinder.
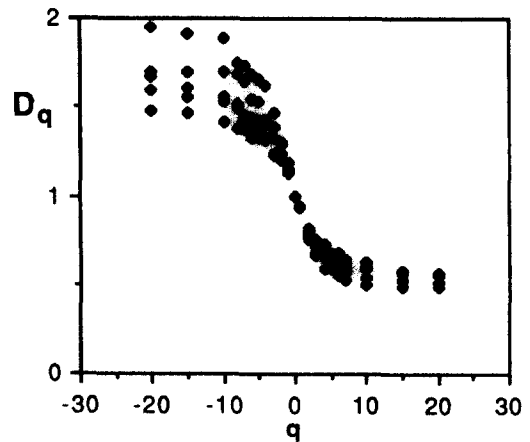

Figure 8. Generalized dimensions D_q as a function of q for 5 different subsets S(j) of the dissipation field measured in the surface layer of the atmosphere.

To quantify the fluctuations of the D_q from one S(j) to another, we present in figure 9 some measured probability densities for 3 different values of q, namely, $D_{20}(j)$, $D_2(j)$ and $D_{-20}(j)$, with m=45 and n= 30, measured in the case of wake turbulence (flow conditions as in Table 1). The standard deviations of the distributions are 0.068, 0.054 and 0.117 respectively, and the corresponding mean values being 0.49, 0.79 and 1.72. We conlude that the mean values are representative.
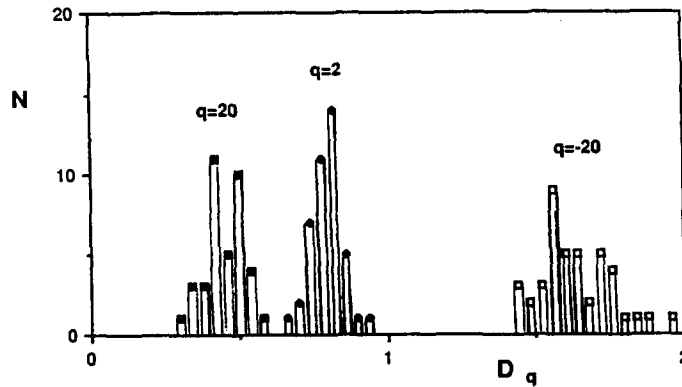
Figure 9. Histograms of the fluctuating generalized dimensions D_q for q=20, 2 and -20, measured for 45 different subsets S(j) of the dissipation field (in the wake behind a cylinder).

Returning to the D_q-curves, we can now use equations (2.13) to obtain $\alpha(q)$ by using central differences to calculate the derivative of $(q-1)D_q$ with respect to q in (2.13) and then calculate its corresponding $f(\alpha)$ using (2.14). Figures 10 to 13 show the multifractal spectra obtained from figures 5 to 8. We draw attention to the fact that we discarded points for which $f(\alpha) < 0$ or $f''(\alpha) > 0$. The former unphysical result occurs as an artifact of relatively large variability in D_q for high values of $|q|$, and the latter follows from (2.10b).

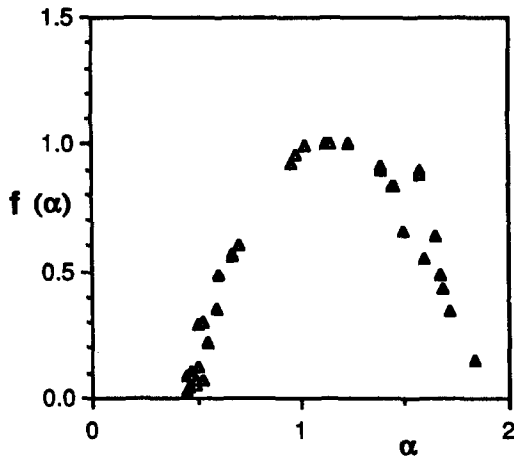

Figure 10. Multifractal spectrum (calculated from results shown in figure 5) of 5 different subsets S(j) of the dissipation field measured in a wind tunnel boundary layer.
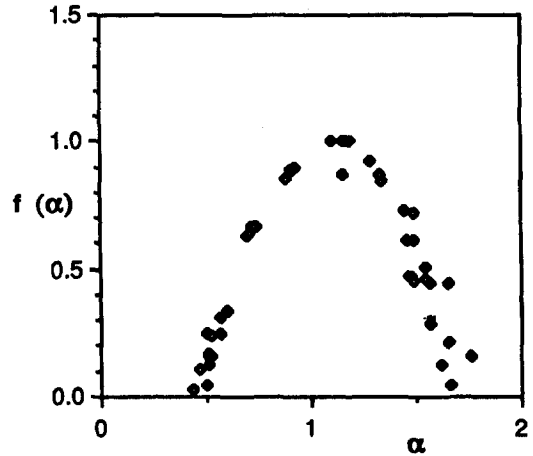
Figure 11. Multifractal spectrum (calculated from results shown in figure 6) of 5 different subsets S(j) of the dissipation field measured in the turbulent flow behind a grid.
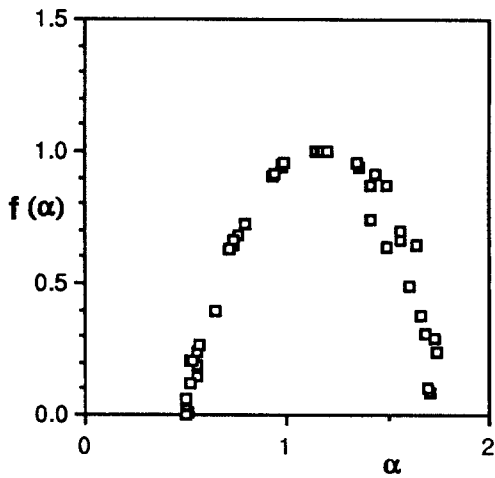
Figure 12. Multifractal spectrum (calculated from results shown in figure 7) of 5 different subsets S(j) of the dissipation field measured in the turbulent wake behind a circular cylinder.
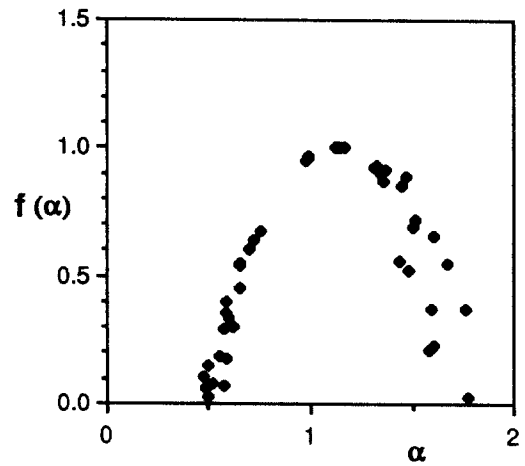

Figure 13. Multifractal spectrum (calculated from results shown in figure 8) of 5 different subsets S(j) of the dissipation field measured in the surface layer of the atmosphere.

Superposing figures 5 to 8 we obtain figure 14. The continuous line is obtained by averaging all the points. In figure 15 we superposed graphs 9 to 13 and the mean is also plotted as a continuous line. We conclude that this continuous line can be regarded as the mean multifractal spectrum corresponding to linear intersections of the energy dissipation field in fully developed turbulence.
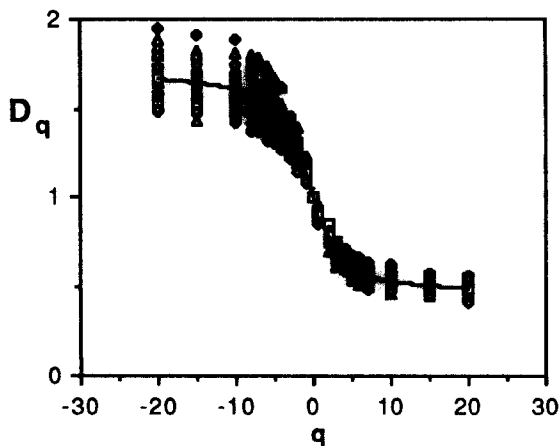

Figure 14. Superposition of the D_q curves shown in figures 5 to 8. The mean is plotted as the continuous line.
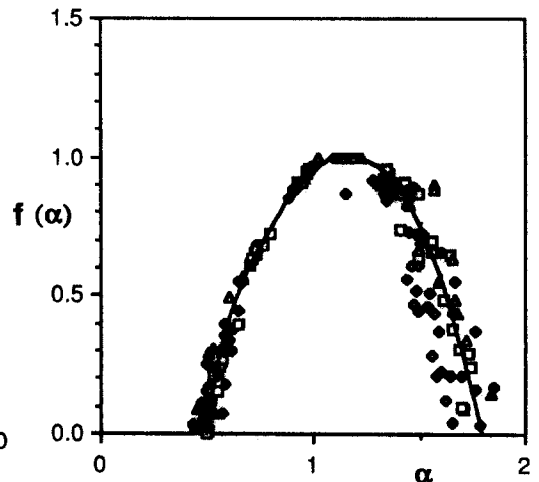

Figure 15. Superposition of the multifractal spectra shown in figures 10 to 13. The mean in plotted as a continuous line.

Some general properties of the measured multifractal spectrum deserve specific comments. Its shape is fairly symmetric and it intersects the α-axis at $\alpha_{min} = 0.51$ and at $\alpha_{max} = 1.78$. The maximum of the curve occurs at $f(\alpha_0)=1$ for $\alpha_0 = 1.117$. There we have $df/d\alpha = 0$, that is $q=0$ from (2.10b), and the corresponding value of $f(\alpha_0)$ is the fractal dimension D_0 of the multifractal set. Our measurements therefore imply that $D_0 = 1$, that is that the metric support of the dissipation field is the embedding space itself: There is at least 'some' dissipation everywhere, even at high Reynolds numbers. This conclusion requires additional comment, since it seems to contradict the fact that the total dissipation has to remain finite. If there are singularities in the dissipation field, that is, field points exist for which equation (2.5) holds, then they have to be on a support of measure zero in order to keep the total dissipation finite. That argument is completely valid in the range $0 < \alpha \leq 1$. For $\alpha > 1$, however, the 'singularities' really correspond to 'holes', that is ε_r tends to zero as r tends to zero, and since our measured α_0 is greater than 1, $f(\alpha_0)=1$ is perfectly consistent with finite total dissipation. From figure 15 we see that $f(1)=0.95$, this means that singularities with $\alpha < 1$ are distributed on fractals (sets with zero measure) of dimensionality less or equal to 0.95, thus satisfying the finiteness of total dissipation.

4. Probability density function of ε_r

4.1 General theory

Let us now consider the problem of obtaining the probability density function of ε_r given its f-α curve.

Let us rewrite equation (2.5) as

$$\varepsilon_r = \varepsilon_L \ (r/L)^{\alpha-1} \tag{4.1}$$

where ε_L is the mean dissipation averaged over a large region of size L. Therefore we can express α as a function of ε_r (except when $\varepsilon_r = 0$ for nonzero r):

$$\alpha = \log(\varepsilon_r/\varepsilon_L) \ / \ \log(r/L) \ + \ 1. \tag{4.2}$$

The probability densities of ε_r and α are related by

$$P_\varepsilon(\varepsilon_r) = P_\alpha(\alpha) \ d\alpha/d\varepsilon_r \ [\ P(\varepsilon_r \neq 0)]^{-1}. \tag{4.3}$$

Here, $P_\alpha(\alpha)$ is the probability density of the variable α and $P(\varepsilon_r \neq 0)$ is the probability that ε_r is non-zero for non-zero r. This is equal to the

probability that a box of size r contains part of the multifractal, and can be written in terms of its fractal dimension D_o as

$$P(\varepsilon_r \neq 0) = c_1 (r/L)^{d-D_o} .$$ (4.4)

Since iso-α sets are fractals, we can write the probability density for α lying between α and $\alpha + d\alpha$ in a box of length r as

$$P_\alpha(\alpha) = c_2 (r/L)^{d - f_d(\alpha)}$$ (4.5)

where c_2 is an arbitrary number that may depend on α but not depend on r. Finally we can write :

$$P_\varepsilon(\varepsilon_r) = C (r/L)^{D_o - f_d[\ln(\varepsilon_r/\varepsilon_L)/\ln(r/L) + 1]} [\varepsilon_r \log(r/L)]^{-1} .$$ (4.6)

Given a specific f-α curve (and supposing that c_2 does not depend on α), one can therefore calculate the probability density of ε_r, which depends on the parameter (r/L). In reality c_2 may depend to some extent on α, and this should be kept in mind in interpreting the results of the following section.

4.2 The lognormal case

Let us expand the f-α curve around its maximum up to second order as

$$f(\alpha) = f(\alpha_o) + (\alpha - \alpha_o) f'(\alpha_o) + 1/2 (\alpha - \alpha_o)^2 f''(\alpha_o) + \ldots\ldots$$ (4.7)

Since $f'(\alpha_o) = 0$ and $f(\alpha_o) = D_o$, we can write

$$f(\alpha) = D_o + (f''(\alpha_o)/2) (\alpha - \alpha_o)^2 .$$ (4.8)

There is still an extremely interesting property of the f-α curve that has to be made use of, and it refers to the behavior of equations (2.13) and (2.14) at q=1. Clearly for q=1 one has

$$\alpha_1 = f(\alpha_1) \qquad \text{and} \qquad df/d\alpha |_{\alpha_1} = 1$$ (4.9 a, b)

where α_1 is given by (2.13) for q = 1. The conditions (4.9) mean that not any parabola with $f''(\alpha) < 0$ can be a valid f-α curve, but that it has to be tangent to the line $f(\alpha) = \alpha$ at $\alpha = \alpha_1$. This property is directly related to the proper behavior of the 'information dimension' D_1 (see Hentschel & Procaccia, 1983). This imposes an additional relation between α_o, D_o, and

$f''(\alpha_0)$. From (4.8) and the first of (2.10b), we have

$$q = df/d\alpha = f''(\alpha_0)(\alpha - \alpha_0).$$

It follows from (4.9b) that

$$\alpha = q/f'' + \alpha_0 \quad \text{and} \quad \alpha_1 = 1/f'' + \alpha_0.$$

Therefore, $f(\alpha_1) = D_0 + 1/(2f''(\alpha_0))$ which, with (4.9b), gives

$$f''(\alpha_0) = 1/[2(D_0 - \alpha_0)]. \tag{4.10}$$

The final expression for the parabolic f-α curve is given, from (4.8), to be

$$f(\alpha) = D_0 - 1/4 \ (\alpha - \alpha_0)^2/(\alpha_0 - D_0). \tag{4.11}$$

Replacing (4.11) in (4.6) and changing the base from r/L to an exponential, we get (after normalization) that $P_\varepsilon(\varepsilon_r)$ is a lognormal distribution with the following parameters (referred to log ε_r):

$$\text{mean} = m = \log \varepsilon_L - (\alpha_0 - 1) \log(L/r), \tag{4.12}$$

$$\text{variance} = \sigma^2 = 2(\alpha_0 - D_0) \log(L/r). \tag{4.13}$$

From the last relation, we infer that the 'lognormal intermittency exponent' (Kolmogorov 1962) is related to the parabolic f-α curve by

$$\mu_{lg} = 2(\alpha_0 - D_0). \tag{4.14}$$

We call this number the 'lognormal intermittency exponent' to distinguish it from the intermittency exponent μ treated in section 7. The latter constant does not invoke lognormality.

Next we address the problem of how the D_q- q curve looks for the lognormal case. Using the result that $\alpha = q/f'' + \alpha_0$, and equation (2.14), we obtain (after some algebra) the result that

$$D_q = D_0 - (\alpha_0 - D_0) q, \tag{4.15}$$

that is, D_q is linear with q, with slope = $-1/2 \ \mu_{lg}$.

Now we want to select the parameters α_0 and D_0 in order to fit our

experimental results. Clearly $D_o = 1$. Selecting α_o from figure 15 corresponds to fitting a straight line at q=0 through the D_q curve in figure 14. A good fit is shown in figure 16 as the continuous line, which transforms to the f-α curve shown in figure 17 also as a continuous line, where the value $\alpha_o = 1.117$ has been used. In figure 16 and 17 we also display the measured mean curves for comparision. It is clear that the fit seems very good in the multifractal spectrum, but is extremely poor in representing the D_q curve for $|q| > 3$. This suggests that the f-α curve is not the best representation of experimental data if one is interested in the high moments. The D_q curve is richer because, in going from the D_q curve to the f-α spectrum, a lot of information has been compressed (and even lost) for high $|q|$; recall that points with $f''(\alpha) > 0$ were discarded.
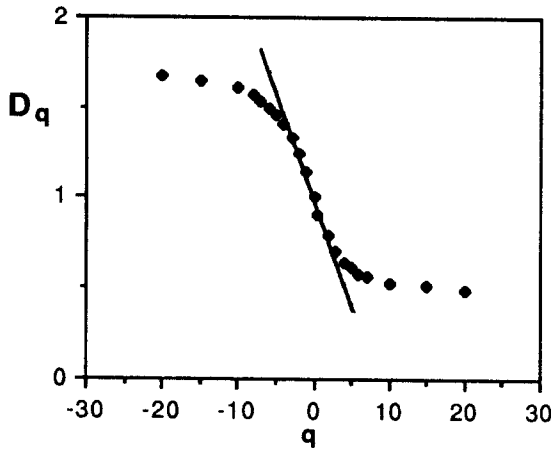

Figure16. Mean experimental D_q curve and linear fit (lognormal approximation) around q=0.
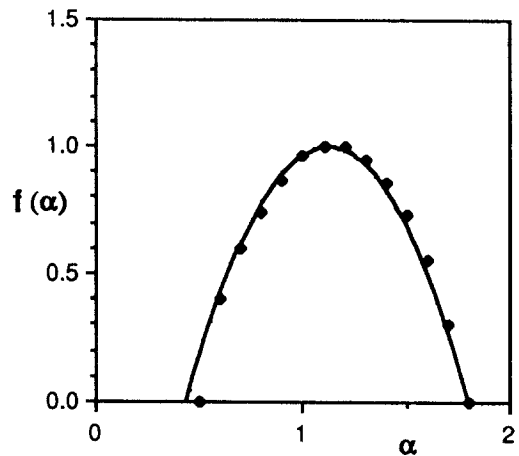
Figure 17. Mean experimental multifractal spectrum and lognormal approximation (continuous line).

Going back to relation (4.14) and replacing the 'measured' value of α_o, we see that $\mu_{lg} = 0.235$, a result that is in remarkable agreement with other extensive measurements of this quantity (Anselmet et al. 1984).

5.Velocity structure functions

Let us now calculate the scaling exponents ξ_p of the moments of velocity differences in fully developed turbulent flows. These exponents are defined by the equation

$$< \delta V_r^p > \ = \ < [V(\underline{x}+\underline{r}) - V(\underline{x})]^p > \ \sim \ r^{\xi_p} \qquad (5.1)$$

Noting from (2.5) that $\varepsilon_r \sim r^{(\alpha - 1)}$, and using (2.3), we can write that $\delta V \sim r^{\alpha/3}$, so that

$$\delta v_r^p \sim r^{\alpha p/3} \tag{5.2}$$

The next step involves space averaging over the entire volume. As before, we change the integration variable to α and we have to weight the integrand by the probability that α lies between α and $\alpha + d\alpha$, that is, by a factor proportional to $r^{d-f_d(\alpha)}$. (Note that since we are averaging we have to weight by probabilities, whereas in section 2 we had to weight by the number of iso-α boxes since we were estimating sums.) Here $f_d(\alpha)$ are the fractal dimensions of "iso-α" sets embedded in d-dimensions. Using again the method of steepest descent and taking the limit of small r, one gets

$$\alpha \, p/3 - f_d(\alpha) + d = \xi_p \tag{5.3}$$

provided that

$$df(\alpha)/d\alpha = p/3 \ . \tag{5.4}$$

Comparing this last identity with the first of (2.10b), we see that $p/3 = q$, and using again the invariance of the codimension under intersection, we can write :

$$\alpha \, p/3 - f(\alpha) + 1 = \xi_p \ . \tag{5.5}$$

Using equation (2.14) we finally conclude

$$\xi_p = (p/3 - 1) D_{p/3} + 1 \ . \tag{5.6}$$

We can now compare experimental results by Anselmet et al. (1984) with inferences from our experimental D_q curve.

The continuous curve in figure 18 corresponds to ξ_p v/s p using equation (5.6) and the continuous D_q curve of figure 14 representing the mean D_q behavior in our experiments. The different symbols in figure 18 correspond to the direct measurement of ξ_p in the experiments of Anselmet et al. (1984). The agreement between the two sets of experimental results is excellent. Thus, the nonlinear behavior of the scaling exponents of velocity differences is included within the multifractal formalism as was proposed originally in Frisch & Parisi (1983), and

developed further by Benzi et al. (1984). We want to draw attention here to the fact that these last authors presented an interesting probabilistic extension of the β-model to simulate a multifractal, where β is now a random variable whose moments can be expressed as a function of ξ_p or equivalently D_q.
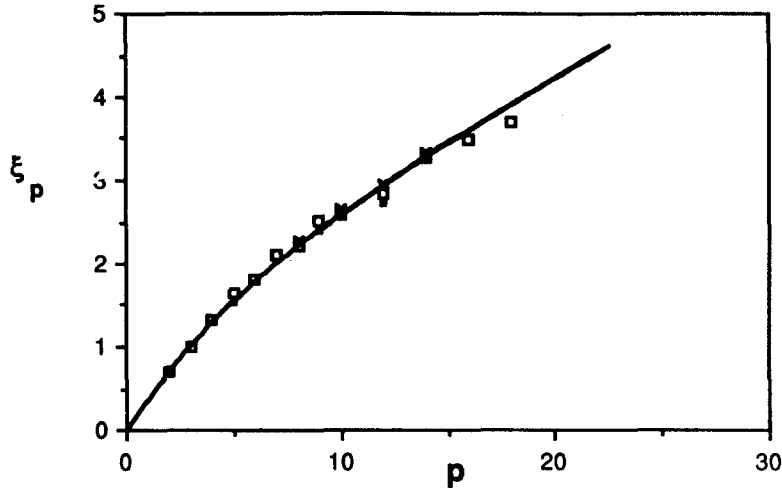

Figure 18. Scaling exponents of velocity structure functions. The continuous curve is obtained using the present experimental results, and the symbols correspond to experiments by Anselmet et al., 1984.

6. Energy spectrum in the inertial range

The kinetic energy carried by eddies of size r can be estimated as

$$W(r) \sim \, < \delta V_r^2 > \; . \tag{6.1}$$

Using equation (5.6) with p=2 we can write in terms of one-dimensional section results as

$$W(r) \sim r^{\,1/3(1-D_{2/3}) \, + \, 2/3} \; . \tag{6.2}$$

In terms of the wavenumber k=1/r this may be written as

$$W(k) \sim k^{\,-2/3 \; -1/3(1-D_{2/3})} \; , \tag{6.3}$$

and the energy density contained in a wavenumber interval dk is   given by

$$E(k) \sim k^{-5/3 \, - \, 1/3(1-D_{2/3})} . \tag{6.4}$$

Thus the famous Kolmogorov -5/3 law is modified by $1/3(1-D_{2/3})$ in the multifractal model. Note that for a homogenous fractal (β-model), $D_{2/3}=D_0$ and the correction is $1/3(1-D_0)$, a result that was first obtained by Mandelbrot (1974).

Since the value of $D_{2/3}$ obtained from our experiments is close to 1 ($D_{2/3}=0.92$), the correction to the -5/3 exponent in (6.4) is negligible; it is experimentally not detectable from power spectra of turbulent velocity signals. This is consistent with the general experimental confirmation of the -5/3 power spectrum in the inertial range of turbulence.

7. Intermittency exponent of the autocorrelation function of ε_r

The autocorrelation function of the local rate of energy dissipation obeys (in the inertial subrange of turbulence) the scaling law

$$< \varepsilon(\underline{x}) \, \varepsilon(\underline{x} + \underline{r}) > \; \sim \; \varepsilon_0^2 \; (r/L)^{- \, \mu} \tag{7.1}$$

where μ is the intermittency exponent already mentioned in section 4. For homogeneous turbulence one can write (Novikov 1971)

$$< \varepsilon(x) \, \varepsilon(x + r) > \; \sim \; < \varepsilon_r^2 > , \tag{7.2}$$

where ε_r is again the energy dissipation averaged over a domain of size r. Now we follow the same arguments as in the preceeding sections for the special case $q = p/3 = 2$ to obtain

$$< \varepsilon_r^2 > \; \sim \; r^{\, 2(\alpha \, -1) \, - \, f_d(\alpha) \, + \, d} \; \sim \; r^{2(\alpha-1) \, - \, f(\alpha) \, +1} \sim r^{2\alpha \, - \, f(\alpha) \, -1} . \tag{7.3}$$

Since (from 2.14) $2\alpha - f(\alpha) = D_2$, we find that

$$< \varepsilon_r^2 > \; \sim \; r^{\, (D_2 \, - \, 1)} . \tag{7.4}$$

From equation (7.1), we have

$$\mu = 1 - D_2 . \tag{7.5}$$

Figure 14 shows that a reasonable estimate for D_2 is $D_2=0.75$, and therefore $\mu=0.25$, which is very close to the value of μ_{lg} obtained in section 4. This is due to the fact that for low moments ($q=2$), the lognormal is a very good

approximation to the actual multifractal distribution.

8. Skewness and the flatness factor of velocity derivatives

We can write from (3.1) and (2.5) that

$$(du_1/dx_1)^2 \sim (\eta/L)^{\alpha-1},$$

where r in (2.5) has been replaced by (η/L) with the understanding that η is the smallest scale of interest in turbulent energy dissipation. Now, noting that $(du_1/dx_1)^2$ is distributed as a multifractal, the average of the m-th power of $(du_1/dx_1)^2$ is given by

$$(\eta/L)^{m(\alpha-1) + 1 - f(\alpha)}.$$

But, from (2.14), $m\alpha - f(\alpha) = (m-1) D_m$. Thus,

$$< (du_1/dx_1)^{2m} > \; \sim \; (\eta/L)^{m(\alpha-1) + 1 - f(\alpha)} \; \sim \; R_\lambda^{1.5(m-1)(1-D_m)}, \tag{8.1}$$

where we have used the fact that $\eta/L \sim R_\lambda^{-1.5}$. Here, R_λ is the Taylor microscale Reynolds number= $u'\lambda/\nu$, u' being the root-mean-square velocity and λ the Taylor microscale.

Defining as usual the skewness S and the flatness factor K of (du_1/dx_1) as

$$S = < (du_1/dx_1)^3 > /< (du_1/dx_1)^2 >^{3/2}$$

$$K = < (du_1/dx_1)^4 > /< (du_1/dx_1)^2 >^2 ,$$

it is easy to see from (8.1) that

$$S \sim R_\lambda^{3/4(1 - D_{3/2})} \quad \text{and} \quad K \sim R_\lambda^{3/2(1 - D_2)} .$$

From figure 14, we estimate that $D_{3/2} = 0.80$ and $D_2 = 0.75$, and hence that

$$S \sim R_\lambda^{0.15} \tag{8.2}$$

and

$$K \sim R_\lambda^{0.38} . \tag{8.3}$$

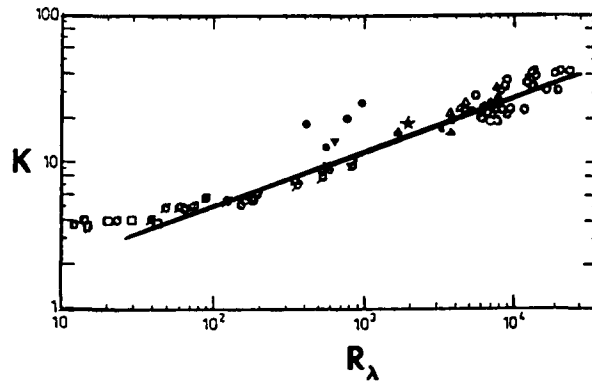Figures 19 and 20 bear out these relations quite satisfactorily.

Figure 20. The skewness of velocity derivatives as a function of Reynods number. The line corresponds to equation (8.2) and the different symbols correspond to experimental data as collected by Van Atta & Antonia (1980).
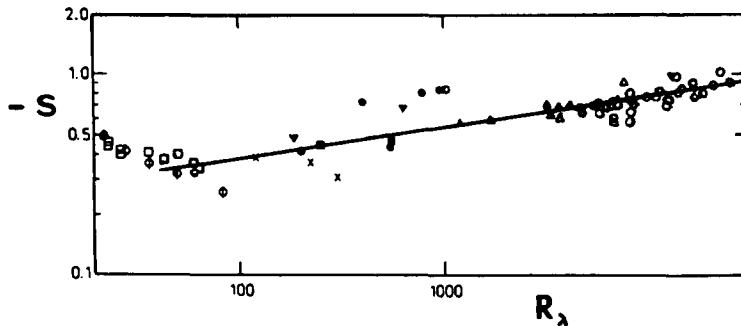

Figure 19. The flatness factor of velocity derivatives as a function of Reynolds number. The line corresponds to equation (8.3) and the different symbols correspond to experimental data as collected by Van Atta & Antonia (1980).

9. Multifractal corrections for the fractal dimension of interfaces

If two species of matter are separated by an interface, the amount M of diffusion of one species from one side of the interface to the other depends on the surface area of the interface, the concentration gradient normal to the surface, and the molecular diffusion coefficient. We shall restrict to cases where the diffusion coefficient is equal to the viscosity coefficient, although extension to non-unity Prandtl and Schmidt numbers is more or less trivial. Using the notion that such interfaces are fractals (Sreenivasan & Meneveau 1986), and that there is a finite inner cut-off at the Kolmogorov scale, we have shown (Sreenivasan 1987) that

$$M \sim R_L^{3/4 \ (D-7/3 \ )} \tag{9.1}$$

where D is the fractal dimension of the interface embedded in three dimensional physical space. The result applies with very little variation to the amount of non-vortical fluid entrained across the vorticity/no-vorticity interface of a turbulent free shear flow. (The boundary layer is a bit more involved, but the final result is no different.)

Now, it is known that the entrainment rate and mixing are independent of Reynolds number if the latter is sufficiently high (the so-called Reynolds number similarity). Invoking this result in the context of (9.1), we get the result that

$$D = 7/3. \tag{9.2}$$

This is very close to the measured value of 2.35 ± 0.05 (Sreenivasan & Meneveau 1986).

In the estimates for **M** which lead to (9.1), it is necessary to determine the concentration gradient which, among other things, depends on the interface thickness. In deriving (9.1), we have used the result that the interface thickness is of the order of η (details of this derivation and other estimates will be published elsewhere). In reality, the Kolmogorov thickness is not a constant because, ε, the dissipation of the turbulent energy, is nonuniform in space. Our limited objective is here is to improve upon (9.2) by making use of the fact that ε is distributed as a multifractal. (We note however that correction due to other factors may be at least as significant.) Without going into details, we present the final result that

$$D = 7/3 + 3/4(1- D_{1/4}) . \tag{9.3}$$

From the multifractal spectrum, we estimate that $D_{1/4}$ is = 0.96, and that the value of D=2.36 from (9.3) is amazingly (perhaps fortutiously) close to the measured mean value of 2.35 quoted above.

10. CONCLUSIONS

We have related the multifractal model of turbulence to direct experimental data and have constructed the f-α curve for the turbulent dissipation field. This curve (in addition to the D_q curve) contains all the information about the scaling properties of the turbulent dissipation field, and can be used to relate several scaling exponents and concepts that lacked a unique and consistent representation in the general turbulence literature.

The present results exemplify the fruitful connections that can be

made between the theory of nonlinear dynamical systems and turbulence. If we consider the qualitative similarity between the vortex-stretching and folding mechanism governed by the N-S equations and the way a simple non-linear map 'organizes' its attractor in phase space, the following procedure might prove interesting :   Given the experimental f-α curve, it is now possible to obtain a lot of information about the properties of a non-linear map that displays the given f-α curve (Feigenbaum et al. 1986). This could lead to a simple map that models how the N-S equations govern the spatial distribution of turbulent dissipation, which may allow further insight on the N-S equations and be useful in a variety of ways (for instance in numerical models of turbulence).

From the experimental and theoretical points of view, there are a great number of further questions to be addressed. Two-dimensional sections of a flow illuminated by thin sheets of laser light in different directions can be analyzed using digital imaging techniques. Extension of the multifractal approach to anisotropic fractals seems a promising task (interesting work in this direction has already been done by Lovejoy & Schertzer, 1985). One can obtain the f-α curve for the dissipation field of a passive scalar, such as temperature or concentration, and compare with the present results. Our efforts continue in these directions.

APPENDIX A

The set of equations (2.12a) and (2.12b) can be used to relate local properties (α) with global ones (D_q and $f(\alpha)$). Here we shall study the relationship between the generalized exponents D_q for an isotropic multifractal and the D_q's of multifractals formed by intersections with lower-dimensional subspaces.

Let us suppose we have an isotropic multifractal F_1 embedded in a d_1-dimensional space S_1. Locally, ε_r and $E_{r,d1}$ can be written as

$$\varepsilon_r \sim r^{\alpha-1} \tag{A.1}$$

$$E_{r,d1} \sim r^{\alpha-1+d_1}, \tag{A.2}$$

where r is again the spatial extent; if F_1 is isotropic, r can be taken in any

direction. Figure A1 illustrates the behavior of ε_r for $d_2 = 2$.

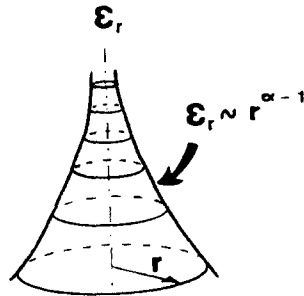

ε_r

$\varepsilon_r \sim r^{\alpha - 1}$

r

Figure A1. Mean dissipation as a function of radial distance in a locally isotropic geometry.

If one is dealing with a probability measure on strange attractors, then $E_{r,d1}$ is the number of points of the attractor that fall in a d_1-dimensional box of size r. In the context of the present work it is the total dissipation of turbulent kinetic energy in such a box.

Suppose that $D_{q,d1}$ and $f_{d1}(\alpha)$ are the sets of generalized dimensions and the multifractal spectrum of F_1. Let us now intersect it with a d_2-dimensional subspace S_2 and form F_2 and suppose that $D_{q,d2}$ and $f_{d2}(\alpha)$ characterize the new set F_2 ($d_2 < d_1$, $d_2 = 1,2...$ and $d_1 = 2,3,..$).

Next we make use of a theorem (Mandelbrot 1983, Mattila 1975 and Marstrand 1954) which, when applied to an iso-α fractal set can be written as

$$f_{d1}(\alpha) \ = \ \max \ \{f_{d2}(\alpha) - d_2 + d_1 \ , \ 0\} \ . \tag{A.3}$$

Let us consider the situation where α is in an interval Λ such that

$$f_{d2} - d_2 + d_1 \ > 0 \tag{A.4}$$

If we write equations (2.12a) and (2.12b) for F_1 and F_2 and use equation (A.3), it can be shown that

$$d_1 - D_{q,d1} \ = \ d_2 \ - D_{q,d2} \tag{A.5}$$

for all $\alpha \in \Lambda$. Equivalently, one can find an interval Q for the values of q such that $\alpha \in \Lambda$.

We conclude that the 'generalized codimensions' $d_i - D_{q,di}$ are almost

surely constant under intersection as long as q ∈ Q. For instance, we can write for $d_1=3$, $d_2=1$ and q ∈ Q

$$D_{q3} = D_{q1} + 2 .$$

(A.6)

Appendix B

Using one single component $(\partial u_1/\partial x_1)^2$ in place of the total dissipation field ε is a common practice, but hardly justified in view of the fact that

$$\varepsilon = \nu \ (\partial u_i/\partial x_j + \partial u_j/\partial x_i)^2$$

consists of several cross terms as well. The situation, though understandable because there is no known method of measuring all components of ε, makes it especially difficult to assess the reasonableness of this common practice. However, for ε_θ, the dissipation of a scalar quantity θ defined as

$$\varepsilon_\theta = \Gamma \ (\partial\theta/\partial x_i)(\partial\theta/\partial x_i) ,$$

all three terms can be measured simultaneously (Sreenivasan et al. 1977). Some assessment of the differences between a single component such as $(\partial\theta/\partial x_1)$ and ε_θ has been made, but not much is known at present about them in the context of the f-α curve. Our preliminary work suggests that no qualitative changes can be expected.

The Taylor's frozen flow hypothesis, which assumes that

$$\partial/\partial t = -U_1 \ \partial/\partial x_1 ,$$

(B.1)

has been the subject of extensive study; U_1 is the mean velocity in the direction x_1. In a recent study, Antonia et al. (1980) have shown that the use of Taylor's hypothesis underestimates the velocity moments (especially the odd-order ones), but that other errors due to neglect of fluctuation velocities in (B.1) are comparable.

Appendix C

The scaling range for negative values of q was generally smaller than for positive q, and did not extend down to r ~ η. This is due to the fact that $\Sigma \ E_\eta^q$ for q<0 is dominated by the low intensity regions, where the finite resolution of the digitizer could become important. However this difficulty dissapears approximately at r ~ 10-20η; E_r then is already the sum of many different E_η and is likely to be dominated by some larger values of E_η far above the digitizer noise.

We verified this plausibility argument with several exactly-solvable two-scale Cantor sets, by adding digitizer noise essentially equivalent to the experimental situation. The same behavior as in the experiment was observed: The scaling range was shortened, but within the available scaling range the correct slopes for D_q were always observed.

REFERENCES:

Antonia, R.A., Phan-Thien, N., & Chambers, A.J. 1980 J. Fluid Mech.**100**, 193

Anselmet, F., Cagne, Y., Hopfinger, E.J. & Antonia, R.A. 1984
          J. Fluid Mech. **140**, 63

Benzi, R. , Paladin, G., Parisi, G. & Vulpiani, A.   1984   J. Phys A **17**, 3521

Feigenbaum, M., Jensen, M.H. & Procaccia, I. 1986   Phys. Rev. Lett. **57**,1507

Frenkiel, F.N. & Klebanoff, P.S.   1975   Boundary-Layer Metereology **8**, 173

Frisch, U. & Parisi, G. 1983   in "Turbulence and Predictability in Geophysical
          Fluid Dynamics and Climate Dynamics". (ed. by M.Ghil, R. Benzi &
          G. Parisi, North-Holland, New York, 1985), p84

Frisch, U., Sulem, P.L. & Nelkin, M.   1978   J. Fluid Mech. **87**, 719

Halsey, T.C., Jensen, M.H., Kadanoff, L.P., Procaccia, I. & Shraiman, B.I. 1986
          Phys. Rev. A **33**, 1141

Hentschel, H.G.E. & Procaccia, I.   1983   Physica **8D**, 435

Kolmogorov, A. N. 1941 C. R. Acad. Sci. U.S.S.R. **30**, 301, 538

Kolmogorov, A. N. 1962 J. Fluid Mech. **13**, 82

Kraichnan, R. H.   1974   J. Fluid Mech. **62**, 305

Lovejoy, S. & Schertzer, D.   1985   Water Resources Research   **21**, 1233

Mandelbrot, B.B   1972   In 'Statistical Models and Turbulence'
          (ed. M. Rosenblatt & C. Van Atta, Springer),   p333

Mandelbrot, B.B.   1974   J. Fluid Mech.   **62**, 331

Mandelbrot, B.B. 1983   The Fractal Geometry of Nature
          (Freeman, San Fransisco)

Marstrand, J. M.   1954   London Math. Soc. **3**, 257

Mattila, P.   1975   Ann. Acad. Sci. Fenn.   Series A Math.   227

Novikov, E.A.   1971   Prikl. Math. Mech. **35**, 266

Sreenivasan, K.R   1984   Phys. Fluids   **27**, 1048

Sreenivasan, K.R.   1987   The Stanley Corrsin memorial lecture, Johns
          Hopkins University, Baltimore.

Sreenivasan, K.R. & Meneveau, C.   1986   J. Fluid Mech. **173**, 357

Sreenivasan, K.R., Antonia, R.A. & Dahn, H.Q.   1977   Phys. Fluids **20**, 1238

Sreenivasan, K.R., Chambers, A.J. & Antonia, R.A. 1978 Boundary-Layer
          Metereology **14**, 341

Van Atta, C.W. & Antonia, R.A. 1980 Phys. Fluids **23**, 252